Atomic and Electronic Structure of the $BaTiO_3(001)$ $(\sqrt{5} \times \sqrt{5})R26.6°$ Surface Reconstruction

John Mark P. Martirez,[1] Erie H. Morales,[2] Wissam A. Saidi,[3] Dawn A. Bonnell,[2] and Andrew M. Rappe[1]

[1]*The Makineni Theoretical Laboratories, Department of Chemistry, University of Pennsylvania, Philadelphia, Pennsylvania 19104-6323, USA*

[2]*Department of Materials Science and Engineering, University of Pennsylvania, Philadelphia, Pennsylvania 19104-6202, USA*

[3]*Department of Chemical and Petroleum Engineering, University of Pittsburgh, Pittsburgh, Pennsylvania 15261, USA*

(Received 20 August 2012; published 20 December 2012)

This contribution presents a study of the atomic and electronic structure of the $(\sqrt{5} \times \sqrt{5})R26.6°$ surface reconstruction on $BaTiO_3$ (001) formed by annealing in ultrahigh vacuum at 1300 K. Through density functional theory calculations in concert with thermodynamic analysis, we assess the stability of several $BaTiO_3$ surface reconstructions and construct a phase diagram as a function of the chemical potential of the constituent elements. Using both experimental scanning tunneling microscopy (STM) and scanning tunneling spectroscopy measurements, we were able to further narrow down the candidate structures, and conclude that the surface is either TiO_2-$Ti_{3/5}$, TiO_2-$Ti_{4/5}$, or some combination, where Ti adatoms occupy hollow sites of the TiO_2 surface. Density functional theory indicates that the defect states close to the valence band are from Ti adatom $3d$ orbitals ($\approx$1.4 eV below the conduction band edge) in agreement with scanning tunneling spectroscopy measurements showing defect states 1.56 ± 0.11 eV below the conduction band minimum (1.03 ± 0.09 eV below the Fermi level). STM measurements show electronic contrast between empty and filled states' images. The calculated local density of states at the surface shows that Ti $3d$ states below and above the Fermi level explain the difference in electronic contrast in the experimental STM images by the presence of electronically distinctive arrangements of Ti adatoms. This work provides an interesting contrast with the related oxide $SrTiO_3$, for which the (001) surface $(\sqrt{5} \times \sqrt{5})R26.6°$ reconstruction is reported to be the TiO_2 surface with Sr adatoms.

DOI: 10.1103/PhysRevLett.109.256802 PACS numbers: 73.20.−r, 68.35.Md, 68.47.Gh, 68.37.Ef

The last decade has seen a resurgence of interest in ferroelectric compounds, due in a large part to recent developments in materials processing that enable new materials properties. Examples include strain controlled ferroelectric coupling [1], polarization controlled surface reactions [2,3], surface chemical control of polarization [4,5], and multiferroic behavior [6]. Surface atomic and electronic structure is a crucial parameter that influences these phenomena, and although the surface science of transition metal oxides is a long-standing field, its application to ferroelectric compounds has been limited. $BaTiO_3$ is considered the prototypical ferroelectric perovskite compound and a model system on which to examine ferroelectric interactions, yet, it is only recently that surface reconstructions have been observed on the (001) surface [7–10]. The determination of the detailed geometric and electronic structure of $BaTiO_3$ (001) is a precursor to understanding interactions at the surface of this compound and of ferroelectric materials in general.

Experimental evidence shows that $BaTiO_3$ undergoes a series of surface reconstructions with (1×1), (2×1), $c(2 \times 2)$, $(\sqrt{5} \times \sqrt{5})R26.6°$, (3×1), (3×2), and (6×1) periodicity at increasing annealing temperatures in highly reducing conditions [8]. The identity of the $(\sqrt{5} \times \sqrt{5})R26.6°$ is also believed to be of the TiO_2-Ti_x type, because experimentally the (3×1) TiO_2-$Ti_{2/3}$ forms under similar experimental conditions [8]. However, the $(\sqrt{5} \times \sqrt{5})R26.6°$ reconstruction has not been investigated theoretically or experimentally in detail.

The present contribution explores the atomic and electronic structure of the $(\sqrt{5} \times \sqrt{5})R26.6°$ surface theoretically and experimentally using *ab initio* density functional theory (DFT) and scanning tunnelling techniques [scanning tunneling microscopy (STM) and scanning tunneling spectroscopy (STS)]. We examine many structures and compositions with the same periodicity to identify the experimentally observed surface structures. Our DFT results explain the electronic contrast in STM images, and the surface atomic state contributions to the valence and conduction bands, which are corroborated by STS measurements. The surface model, consistent with thermodynamic stability analysis, confirms a TiO_2 with Ti adatom surface.

$BaTiO_3$ single crystals are (001) oriented and one side polished. The single crystal is radiatively heated in UHV (pressure of 2×10^{-10} Torr), effectively reducing it and changing its color to either dark blue or black [11]. After sputtering at 1 kV and 1 μA for 20 minutes [12] and

two UHV annealing steps at 1000 K and 1300 K, we obtain the desired reconstruction. STS measurements are performed by measuring $I - V$ curves from -3 to 3 V, with the feedback loop turned off in UHV conditions. See the Supplemental Material for details on the experimental procedure [13].

The surfaces are simulated using slabs with 6-7 atomic layers with the in-plane supercell periodicity fixed at $4.00 \times \sqrt{5}$ Å, where 4.00 Å is the $BaTiO_3$ experimental lattice constant, a. The DFT calculations are performed using the Quantum ESPRESSO [14] package and the Perdew-Burke-Ernzerhof form of the generalized gradient approximation. The core electronic states of the elements were described using norm-conserving pseudopotentials [15–17], generated using the OPIUM code [18]. We did spin-polarized DFT + U [19] ($U = 4.9$ eV) calculations for the electronic structure studies. Further details about the calculations are provided in the Supplemental Material [13].

Approximately 50 surface structures with $(\sqrt{5}\times\sqrt{5})R26.6°$ symmetry, resulting from the introduction of oxygen vacancies on both BaO and TiO_2 surfaces, and adatoms (Ba and Ti) and Ti_xO_y-layers on the TiO_2 surface, were studied. The construction of the phase diagram is described in the Supplemental Material [13].

STM empty state [Fig. 1(a)] and filled state [Fig. 1(b)] images have atomically resolved features corresponding to the periodicity of the $(\sqrt{5} \times \sqrt{5})R26.6°$ surface reconstruction previously observed in $BaTiO_3$ (001) single crystals [8]. Both Figs. 1(a) and 1(b) show white agglomerates that could be composed of BaO-like, BaO_2, or $BaTiO_3$ [20]. Additionally, both figures have the same periodicity; however, the latter exhibits contrast that resembles a mesh whereas the former presents sharper circular atomic features. A representative experimental local density of states (LDOS) obtained from an $I - V$ curve (Fig. S1, Supplemental Material [13]) in Fig. 2(a) was measured on a $(\sqrt{5} \times \sqrt{5})R26.6°$ surface. The values shown are average values drawn from several x-y measurements. The onset of the conduction band minimum is located 0.59 eV above the Fermi level (E_F), and thus the bulk gap is roughly estimated to be from -2.6 to 0.59 eV since the bulk band gap energy is 3.2 eV [21,22]. The $I - V$ curve has negative static conductance that produces an extra gap from 1.51 to 1.86 eV above E_F in Fig. 2(a) which is not an artifact and will be analyzed in context with other $BaTiO_3$ surface reconstructions in a future publication [23]. The energy between the top of the defect states and the conduction band minimum is 1.56 ± 0.11 eV, which is less than the bulk band gap. STS measures the local electronic structure, thus, having states below E_F and in the gap indicates that surface Ti atoms are indeed reduced. The surface states located 1.03 ± 0.09 eV below E_F are attributed to Ti $3d^{3+}$ and also are observed 0.9 eV below E_F in ultraviolet photoelectron spectroscopy measurements [24]. The Ti $3d^{3+}$ surface states seen in our study are in close agreement with previous STS measurements on a surface addressed as the multiple of $(\sqrt{5} \times \sqrt{5})R26.6°$ where defect states located at 0.8 and 1.2 eV below E_F have also been observed [7,25]. The Ti $3d$–derived states are a common constituent of the electronic structures of titanates. They are, for example, observed in TiO_2 [26,27] approximately 1 eV below E_F. Additionally, the $(\sqrt{5} \times \sqrt{5})R26.6°$ reconstruction occurs in $SrTiO_3$ and shows similar defect states at approximately 1.2 eV below E_F, see, for example, Ref. [28].

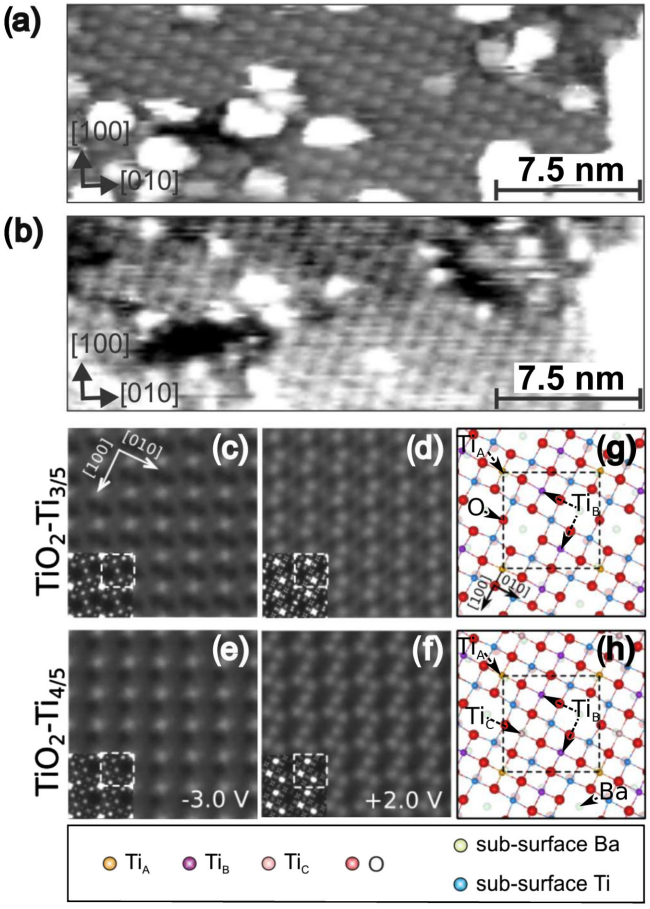

FIG. 1 (color online). Experimental and calculated STM images of $BaTiO_3$ (001) $(\sqrt{5} \times \sqrt{5})R26.6°$ surface. (a) Empty-state image at bias -3.02 V and 0.17 nA, 30 nm × 10 nm. (b) Filled-state image at bias 2.09 V and 0.17 nA, 30 nm × 10 nm. Simulated STM [30]; (c) and (d) are the empty (3 eV above E_F) and filled (2 eV below E_F) state images for TiO_2-$Ti_{3/5}$, respectively. (e) and (f) are the empty and filled state images for TiO_2-$Ti_{4/5}$, respectively. The white dash-lined squares denote the $(\sqrt{5} \times \sqrt{5})R26.6°$ unit, while the lower left insets are the raw images prior to computational smearing to mimic the finite tip resolution. (g) and (h) are the ball-and-stick models of $(\sqrt{5} \times \sqrt{5})R26.6°$ TiO_2-$Ti_{3/5}$ and TiO_2-$Ti_{4/5}$ reconstructions, with dashed lines denoting the $\sqrt{5} \times \sqrt{5}$ super cell. Large spheres: O; small spheres: Ti.

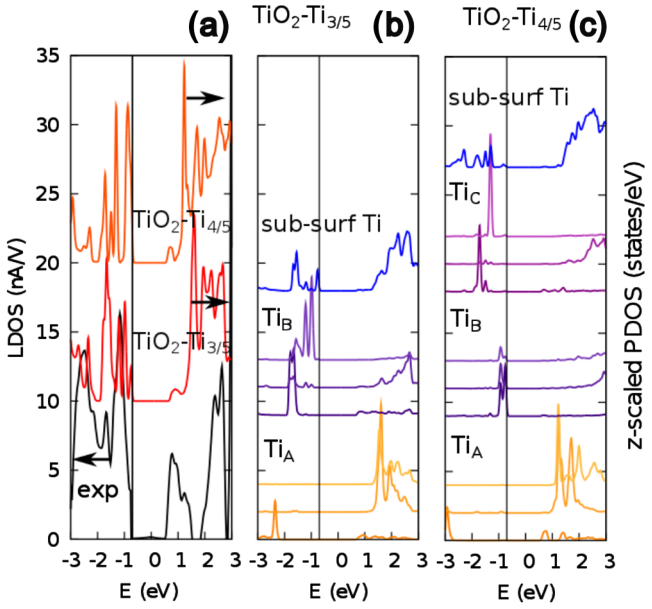

FIG. 2 (color online). Experimental and calculated LDOS of $BaTiO_3$ (001) $(\sqrt{5}\times\sqrt{5})R26.6°$ surface. (a) Experimental surface LDOS and calculated z-scaled projected densities of states (PDOS) [31] of $(\sqrt{5}\times\sqrt{5})R26.6°$ TiO_2-$Ti_{3/5}$ and TiO_2-$Ti_{4/5}$. The valance band maxima (VBM) of the experimental and calculated LDOS are aligned. (b) and (c) PDOS for Ti species found on the surface. The sets of three lines for each Ti adatom (Ti_A, Ti_B, and Ti_C) correspond to $d_{x^2-y^2}+d_{xy}$, $d_{xz}+d_{yz}$, and d_{z^2}, from top to bottom (lightest to darkest shade). For subsurface Ti (found on the underlying TiO_2), the sum of the contribution of all sub-surface Ti states are shown. Some of the spectra are shifted along the y axis for clarity.

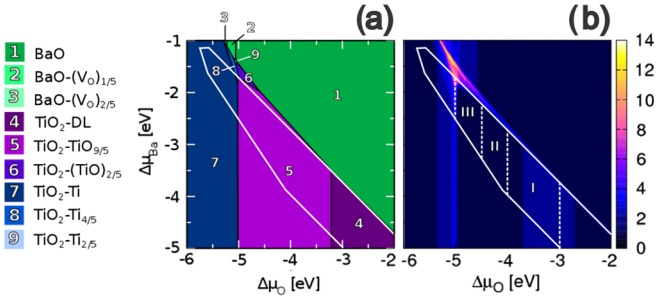

FIG. 3 (color online). (a) Phase diagram generated from first-principles thermodynamic calculations as a function of the relative chemical potential of Ba and O. The white solid lines bound the stability region of $BaTiO_3$ relative to the secondary phases [29] at 1300 K. DL and V_O refer to the double layer structure and surface oxygen vacancy, respectively. (b) Surface phase population where we count the number of surface phases whose energies are within 0.10 eV/primitive unit cell of the lowest energy structure. Regions I to III correspond to $\log[p_{O_2}(\text{torr})]$ in the range of -9 to -17, -17 to -20, and -20 to -24, respectively. The experiment is believed to be between $\log[p_{O_2}(\text{torr})] = -10$ to -27 [8].

The first principles surface phase diagram for surfaces with $(\sqrt{5}\times\sqrt{5})R26.6°$ symmetry is shown in Fig. 3(a). The upper right corner is dominated by BaO and BaO-derived (BaO with O vacancy) surfaces, while the lower left corner contains TiO_2-derived surfaces: the TiO_2 double layer structure (TiO_2 DL), partially reduced TiO_2 DL (TiO_2-$TiO_{9/5}$), and Ti and TiO covered TiO_2 surfaces. The region of stability of $BaTiO_3$ at 1300 K with respect to other secondary phases [29], bordered by the white solid line, runs across the TiO_2-derived surfaces. Given the high temperature conditions of the experiment and the small free energy error due to neglect of entropic contributions from the surface, Fig. 3(b) shows the number of surface phases whose energies are within 0.10 eV per primitive unit cell ($\approx k_BT$) of the lowest energy surface, at any Ba and O chemical potentials.

Within the bulk stability boundary at 1300 K, several surface phases are possible as suggested by the stability analysis represented in Figs. 3(a) and 3(b) (see Supplemental Material for the complete list [13]). We calculated the surface LDOS, and empty and filled state STM images for TiO_2 DL, TiO_2-$TiO_{9/5}$ (owing to their wide range of stability), TiO_2-$Ti_{1/5}$ to TiO_2-$Ti_{4/5}$, and TiO_2-$Ba_{1/5}$ and TiO_2-$Ba_{2/5}$ (TiO_2-$Sr_{1/5}$ having being proposed for the $SrTiO_3$(001) $(\sqrt{5}\times\sqrt{5})R26.6°$ reconstruction). The TiO_2-$Ti_{3/5}$ and TiO_2-$Ti_{4/5}$ proved to be most consistent with both the experimental LDOS spectrum and the STM images, and are identified as stable and close in energy by the DFT-thermodynamic calculations, and thus will be discussed here in more detail. For the structure, calculated LDOS and STM images of other phases, see the Supplemental Material [13].

The ball-and-stick models for $(\sqrt{5}\times\sqrt{5})R26.6°$ TiO_2-$Ti_{3/5}$ (hereafter TiO_2-$Ti_{3/5}$) and $(\sqrt{5}\times\sqrt{5})R26.6°$ TiO_2-$Ti_{4/5}$ (hereafter TiO_2-$Ti_{4/5}$) are shown in Figs. 1(g) and 1(h). In both surfaces, Ti adatoms are situated at the hollow sites of the TiO_2 surface. For TiO_2-$Ti_{3/5}$, each Ti adatom has two Ti adatom neighbors and are arranged in a zigzag pattern where one type (Ti_A, yellow spheres) has its neighbors in a straight line, while the other (Ti_B, purple spheres) has its neighbors 90° to each other. In the case of TiO_2-$Ti_{4/5}$, all Ti adatoms have the same number of Ti-adatom neighbors and neighbors' orientation. However, their electronic structures are different, thus resulting in different appearance in the empty and filled STM images, we annotate them as Ti_A (yellow spheres), Ti_B (purple spheres), and Ti_C (pink spheres).

Calculated empty and filled state STM images [30] of TiO_2-$Ti_{3/5}$ and TiO_2-$Ti_{4/5}$ are shown in Figs. 1(c)–1(f). For TiO_2-$Ti_{3/5}$, the empty state image has bright spots spaced $\sqrt{5}a$ from each other, corresponding to Ti_A adatoms. In the filled state image, a pair of bright spots corresponding to the Ti_B adatoms gives a columnar feature, where the columns are spaced $\sqrt{5}a$ apart. For TiO_2-$Ti_{4/5}$, the empty state image also has

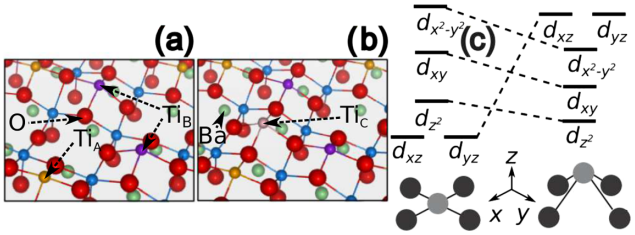

FIG. 4 (color online). A perspective view of the surface structure of $(\sqrt{5}\times\sqrt{5})R26.6°$ TiO_2-$Ti_{3/5}$ (a) and TiO_2-$Ti_{4/5}$ (b) showcasing the oxygen cage geometry of the Ti adatoms, see Figs. 1(g) and 1(h) for legend. (c) Crystal field splitting profile for square-planar (left) and distorted square-planar (right) geometries.

bright spots spaced $\sqrt{5}a$ from each other, associated with Ti_A. The filled state image shows three prominent continuous spots per unit-cell associated with Ti_B and Ti_C, with slight distinction between the shape of their contribution as shown in its inset STM.

The calculated local and projected densities of states [31] for the surfaces indicate that most of the states near E_F (above and below) are derived from d states of Ti adatoms, as shown in Figs. 2(b) and 2(c). Ti_A adatoms compose most of the conduction band while Ti_B and Ti_C adatoms are mostly filled and are found in the energy gap. The LDOS for TiO_2-$Ti_{3/5}$ and TiO_2-$Ti_{4/5}$ have peaks at $\approx 1.44 \pm 0.01$ eV and $\approx 1.45 \pm 0.01$ eV below the surface conduction band, respectively, within the experimental uncertainty. The projected density of states explain the contrast between filled and empty state images, where Ti_A adatoms show in the empty state image while Ti_B and Ti_C show more prominently in the filled state image.

Annealing at extremely high temperature and UHV conditions is a reducing environment, increasing the metal cation-to-oxygen ratio at the surface and changing the Ba:Ti cation ratio as well. The experimental conditions are believed to be such that BaO forms surface agglomerates, which manifest as white cloud-like features in the STM images. Further, the experiment is estimated to be between $\log[p_{O_2}(\text{torr})] = -10$ and -27, where the UHV base pressure serves as the upper limit, while the water partial pressure defines the lower limit [8]. The phase diagram [Fig. 3(a)] predicts the stability of TiO_2-$Ti_{4/5}$ at a point where BaO precipitates and at about $\Delta\mu_O = -5$ eV ($\log[p_{O_2}(\text{torr})] = -24$), where, according to Fig. 3(b), a wide variety of phases may coexist at a 0.10 eV/primitive-unit-cell surface energy window. Despite possible coexistence, we assign the consistency of the $(\sqrt{5}\times\sqrt{5})R26.6°$ surface reconstruction to be of the TiO_2-Ti_x type, based on the experimental STM and STS and computed STM images and LDOS spectra.

In both TiO_2-$Ti_{3/5}$ and TiO_2-$Ti_{4/5}$, the Ti adatoms have distorted square planar geometries, where adatoms are relaxed away from the bulk relative to the coordinating O atoms [Figs. 4(a) and 4(b)]. Due to this distortion, the crystal field splitting is found to resemble a compromise between the splitting in a square-planar and in a square-antiprismatic geometry. The crystal field splitting profiles are shown in Fig. 4(c), where the distortion leads to the stabilization of the d_{z^2}, d_{xy} and $d_{x^2-y^2}$ orbitals and destabilization of the d_{yz} and d_{xz} orbitals.

The occupied states for both surfaces are mostly derived from the d_{z^2} orbitals of Ti_A and Ti_B (and Ti_C in the case of TiO_2-$Ti_{4/5}$), and d_{xy} and $d_{x^2-y^2}$ orbitals of Ti_B (Ti_C in the case of TiO_2-$Ti_{4/5}$). In the calculated STM images, Ti_B and Ti_C adatoms exhibit the most intense signal in the $+2$ V tip bias image, where the d_{z^2}, d_{xy} and $d_{x^2-y^2}$ derived states are sampled. In the -3 V tip bias, the strongest response comes from Ti_A since most of the bands above E_F are derived from d orbitals of Ti_A. Although Ti_A has its d_{z^2} state partially occupied, Ti_B and Ti_C have more occupied d states below E_F, making them more prominent in the filled state images. Therefore, the STM image of empty states shows the distinctive atomic features which are due to Ti_A, and the filled state image is better described by a mesh or columnar feature produced by Ti_B and Ti_C as described above. The compelling resemblance of the experimental and calculated STM images is the consequence of the different electronic structure of the Ti adatoms producing filled and empty defect states in the gap.

$SrTiO_3$ (001) is chemically similar to $BaTiO_3$ (001) and also reconstructs into $(\sqrt{5}\times\sqrt{5})R26.6°$. The surface has been proposed to be TiO_2 terminated with ordered Sr adatoms at 0.20 atoms per unit cell coverage ($\theta = 0.20$, TiO_2-$Sr_{1/5}$) [32–34]. Due to the common perovskite crystal structure and cationic oxidation state of $BaTiO_3$ and $SrTiO_3$ (001) we anticipate that our results are similar for both oxides at the $(\sqrt{5}\times\sqrt{5})R26.6°$ surface. The work of Kubo *et al.* presents DFT calculations with LDOS [32–34] but does not explore the thermodynamic stability of a Sr adatom surface relative to other surfaces. Our calculations, on the other hand, explore systematically several $(\sqrt{5}\times\sqrt{5})R26.6°$ surface phases. In view of similarities between $BaTiO_3$ and $SrTiO_3$, we suggest further study of the composition and structure of the $SrTiO_3$ (001) $(\sqrt{5}\times\sqrt{5})R26.6°$ surface reconstruction.

The authors would like to acknowledge the following funding agencies: J. M. P. M. was supported by the Air Force Office of Scientific Research, Air Force Materiel Command, USAF, under Grant No. FA9550-10-1-0248. A. M. R. was supported by the DOE Office of Basic Energy Sciences, under Grant No. DE-FG02-07ER15920. W. A. S. was supported by the Office of Naval Research, under Grant No. N00014-12-1-1033. Computational support was provided by the High Performance Computing Modernization Program (HPCMO) of the US DOD and the NERSC of the DOE. E. H. M. and D. A. B. would like to acknowledge the support from the National Science Foundation Grants No. DMR0805174 and 1206563.

[1] D. G. Schlom, L. Q. Chen, C. B. Eom, K. M. Rabe, S. K. Streiffer, and J. M. Triscone, Annu. Rev. Mater. Res. **37**, 589 (2007).

[2] A. M. Kolpak, I. Grinberg, and A. M. Rappe, Phys. Rev. Lett. **98**, 166101 (2007).

[3] D. Li, M. H. Zhao, J. Garra, A. Kolpak, A. Rappe, D. A. Bonnell, and J. M. Vohs, Nat. Mater. **7**, 473 (2008).

[4] D. D. Fong, A. M. Kolpak, J. A. Eastman, S. K. Streiffer, P. H. Fuoss, G. B. Stephenson, C. Thompson, D. M. Kim, K. J. Choi, C. B. Eom, I. Grinberg, and A. M. Rappe, Phys. Rev. Lett. **96**, 127601 (2006).

[5] M. J. Highland, T. T. Fister, D. D. Fong, P. H. Fuoss, C. Thompson, J. A. Eastman, S. K. Streiffer, and G. B. Stephenson, Phys. Rev. Lett. **107**, 187602 (2011).

[6] R. Ramesh and N. Spaldin, Nat. Mater. **6**, 21 (2007).

[7] H. Bando, T. Shimitzu, Y. Aiura, Y. Haruyama, K. Oka, and Y. Nishihara, J. Vac. Sci. Technol. B **14**, 1060 (1996).

[8] A. M. Kolpak, D. Li, R. Shao, A. M. Rappe, and D. A. Bonnell, Phys. Rev. Lett. **101**, 036102 (2008).

[9] A. M. Kolpak, Ph.D. thesis, University of Pennsylvania, Philadelphia, Pennsylvania, (2007).

[10] N. Iles, F. Finocchi, and K. Driss Khodja, J. Phys. Condens. Matter **22**, 305001 (2010).

[11] D. Aberdam, G. Bouchet, and P. Ducros, Surf. Sci. **27**, 559 (1971).

[12] A. Berlich, H. Strauss, C. Langheinrich, A. Chass, and H. Morgner, Surf. Sci. **605**, 158 (2011).

[13] See Supplemental Material at http://link.aps.org/supplemental/10.1103/PhysRevLett.109.256802 for further details about the experiment and calculations, experimental *I-V* curve, ball-and-stick models, simulated STM, and z-scaled PDOS.

[14] P. Giannozzi *et al.* J. Phys. Condens. Matter **21**, 395502 (2009).

[15] A. M. Rappe, K. M. Rabe, E. Kaxiras, and J. D. Joannopoulos, Phys. Rev. B **41**, 1227 (1990).

[16] N. J. Ramer and A. M. Rappe, Phys. Rev. B **59**, 12471 (1999).

[17] I. Grinberg, N. J. Ramer, and A. M. Rappe, Phys. Rev. B **63**, 201102(R) (2001).

[18] http://opium.sourceforge.net.

[19] M. Cococcioni and S. de Gironcoli, Phys. Rev. B **71**, 035105 (2005).

[20] U. Cord and R. Courths, Surf. Sci. **152-153**, 1141 (1985).

[21] M. Cardona, Phys. Rev. **140**, A651 (1965).

[22] M. DiDomenico and S. H. Wemple, Phys. Rev. **166**, 565 (1968).

[23] E. H. Morales and D. A. Bonnell (unpublished).

[24] R. Courths, Phys. Status Solidi B **100**, 135 (1980).

[25] T. Shimizu, H. Bando, Y. Aiura, Y. Haruyama, K. Oka, and Y. Nishihara, Jpn. J. Appl. Phys. **34**, L1305 (1995).

[26] Z. Klusek, S. Pierzgalski, and S. Datta, Appl. Surf. Sci. **221**, 120 (2004).

[27] M. Batzill, K. Katsiev, D. Gaspar, and U. Diebold, Phys. Rev. B **66**, 235401 (2002).

[28] H. Tanaka, T. Matsumoto, T. Kawai, and S. Kawai, Jpn. J. Appl. Phys. **32**, 1405 (1993).

[29] Secondary phases considered are BaO_2 (tetragonal), BaO (rock-salt), Ba(*liquid*), TiO_2 (rutile), Ti_2O_3 (corundum), and Ti(hexagonal close-packed).

[30] The 2D STM images are generated from 3D data by summing over-all contribution along the z coordinate multiplied by $\exp(z - z^0)$, where z^0 is the z coordinate of the top most atom on the surface, at given x and y coordinates. Further, the images were Gaussian-blurred to capture the spatial resolution of the experimental STM.

[31] The contribution of atom i to the PDOS is multiplied by an exponential decay function, $\exp(z^i - z^0)$, where z^i and z^0 are the the z coordinate of atom i and of the top most atom on the surface, respectively.

[32] T. Kubo and H. Nozoye, Phys. Rev. Lett. **86**, 1801 (2001).

[33] T. Kubo and H. Nozoye, Surf. Sci. **542**, 177 (2003).

[34] T. Kubo, H. Orita, and H. Nozoye, Phys. Chem. Chem. Phys. **13**, 16516 (2011).